Heliyon 9 (2023) e21699

Contents lists available at ScienceDirect

Heliyon

journal homepage: www.cell.com/heliyon

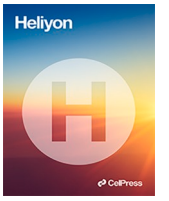

Evaluation of phase change material-graphene nanocomposite for thermal regulation enhancement in buildings

Mohadeseh Amirkhani Khabisi [a], Ghodratollah Roudini, PhD [b,*], Farahnaz Barahuie [c], Hamed Sheybani [d], Muhammad Ibrar [e]

[a] Departmant of Materials Engineering, Tarbiat Modares University, Tehran, Iran
[b] Departmant of Materials Engineering, Faculty of Engineering, University of Sistan and Baluchestan Zahedan, Iran
[c] Faculty of Industry & Mining (Khash), University of Sistan and Baluchestan, Zahedan, Iran
[d] Department of Materials Science and Engineering, Shiraz University of Technology, Shiraz, Iran
[e] Nanotechnology Research Laboratory, Department of Physics, Islamia College Peshawar, Peshawar, Khyber Pakhtunkhwa, Pakistan

ARTICLE INFO

Keywords:
Nanocomposite
Thermal regulation
Nanographene
Thermal conductivity
Phase change materials

ABSTRACT

The growth of high-efficiency phase change material (PCM) nanocomposites with good heat conduction and substantial thermal capacity was of vital significance for practical matters in the sustainable utilization of energy. A novel leakage-proof n-heptadecane-graphene nanocomposite was prepared by a direct impregnation procedure from n-heptadacne as a PCM and nanographene as a skeleton. The creation of shape-stabilized nanocomposite was checked with X-ray diffraction (XRD), Raman, and Fourier transform infrared (FTIR) spectroscopy. The scanning electron microscopy (SEM) analysis illustrated that the n-heptadecane and graphene had favourable compatibility and there was no phase separation and graphene accumulation. Thermal analysis showed that the shape-stabilized nanocomposite not only had a good phase transition enthalpy (101.7 J/g) and n-heptadecane content (45.6 %) but also possessed appropriate thermal stability. The heat conduction of the obtained mesoporous nanocomposite was up to 1.527 W/mK, with a growth of 808 % compared to pure n-heptadecane. Furthermore, the optimized nanocomposite held auspicious thermal reliability, being exposed to 400 thermal cycles. Moreover, the thermoregulation tests demonstrated that the gypsum boards containing optimized nanocomposite showed a slow heat release rate and improved the building temperature profile over only the gypsum board. By virtue of the combination of n-heptadecane and thermal conductive nanographene, the obtained engineered nanocomposite might be regarded as a smart material for energy-conserving and temperature regulation in buildings.

1. Introduction

Materials with the ability to heat storage and release in a controlled manner accomplished a vital function in multitudinous technologies that necessitated thermal energy storage and heat regulation. Phase change materials (PCMs) provided a magnificent approach in that heat was manipulated through phase transitions [1–4]. However, the wide use of commonly used solid−liquid PCMs was hampered by their seepage issue and inherently low heat transfer [5,6]. To address this matter, some high thermal conductive

* Corresponding author.
E-mail address: ghodratollah.roudini@eng.usb.ac.ir (G. Roudini).

https://doi.org/10.1016/j.heliyon.2023.e21699
Received 27 April 2023; Received in revised form 20 October 2023; Accepted 26 October 2023
Available online 29 October 2023

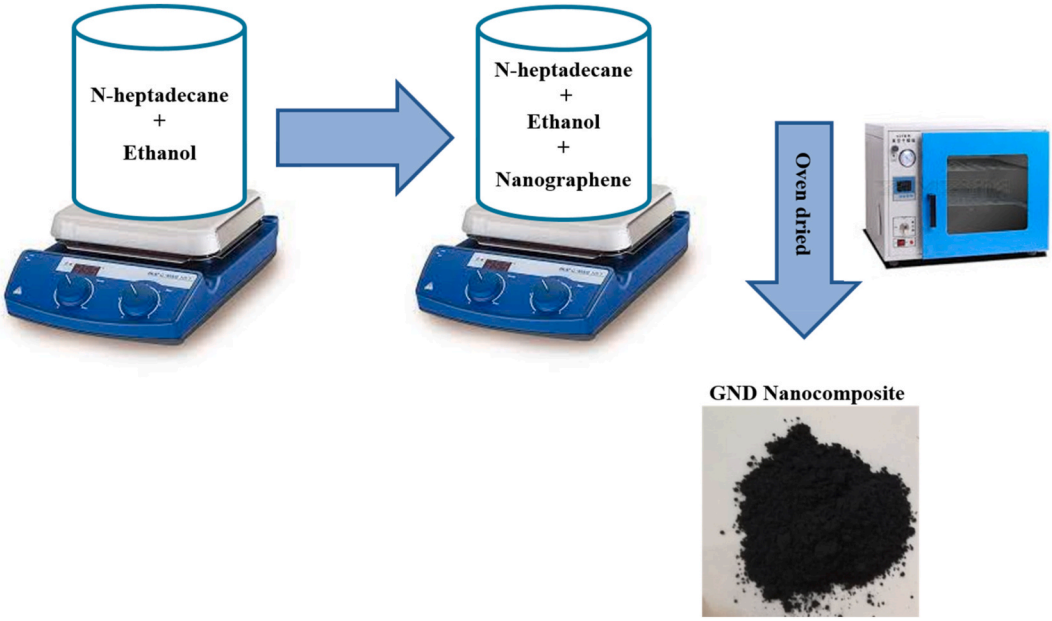

Fig. 1. Schematic illustration of GND nanocomposite production.

nanostructured materials, generally falling into two categories of metal- and carbon-based materials could be introduced into the solid−liquid PCMs as additives to form the PCM nanocomposite [7–9]. These nanoskeleton materials including graphite [10,11], graphene [12,13], metals [14–16], carbon nanotubes [17,18], and others exhibited a promising performance in heat storage, thermal regulation, and construction.

The emerging graphene, a two-dimensional monolayer allotrope of carbon, as a nanoscale material had a broad array of applications in numerous aspects. The high thermal conductivity of graphene made it best for being applied as one of the most proper heat conduction augmenters. By reason of its incredible heat transfer, great dispersion ability, high surface area, and good stability, graphene was conceived to be an impressively propitious material to rise the heat conduction of PCMs [19–21]. Cai et al. used natural latex and graphene aerogel to prepare leakage-proof PCM with high thermal conductivity and multi-energy conversion utilities. The leakage-proof PCM showed excellent photo-sensitive flexibility with a 73.5 % transformation of electric energy into thermal energy at a low driving voltage of 8.0 V and exceptional thermal reliability after 200 heat cycles. Furthermore, the performance of leakage-proof PCM in photo-heat energy alteration was eminent, with a maximum alteration of 91.8 % [22]. Zhou et al. enhanced the heat conduction of polyethylene glycol (PEG) by adding graphene and producing a shape-stabilized PEG-graphene composite. The experimental outcomes evinced that owing to the crosslinking graphene frame and its inherent great heat conduction, the heat flow rate was improved to 116.0 % in the composite (0.381 W/mK) in comparison with PEG (0.238 W/mK) and the weight percent of PEG in the composite was up to 96.0 wt%. Further, the phase change enthalpy of the composite was 223.2 J/g, showing a great energy storage capacity [12]. Jiang et al. made a high thermal conductive PCM composite using 1- hexadecylamine and graphene aerogel by way of melt impregnation. The latent heat and heat conduction of the PCM composite were 1.05 and 1.61 times higher than that of only 1-hexadecylamine with the amount of 284.5 kj/kg and 0.7661 W/mK, respectively [23]. Khannan et al. fabricated *n*-hexacosane--graphene nanocomposite as shape-stabilized PCM. The melting and freezing of nanocomposite were recorded at 57.11 °C with a phase change enthalpy of 154.61 J/g and 49.28 °C with a phase change enthalpy of 147.58 J/g, respectively. The nanocomposite exhibited a heat conduction of 12.63 W/m K, which was raised in comparison to that of *n*-hexacosane of about 0.26 W/m K [24]. Hasbi et al. probed the thermal performance of bio-based phase change materials (BPCMs) including coconut oil, palm wax, and beeswax using TiO_2 and graphene as nano-fillers. The heat conduction of BPCMs boosted between 4 and 46 % in comparison with BPCMs. The nanofillers improved the thermal performance of BPCMs as beeswax nanocomposite had the highest heat conduction of 0.338 W/mK, while coconut oil nanocomposite was the lowest with 0.232 W/mK [25]. Yang et al. demonstrated an efficient combination of thermal conductivity enhancement and convection heat transfer as well as high heat dissipation efficiency (220.8 %) in PCM in the graphene aerogel composite [26]. He et al. designed a shape-stabilized PCM based on paraffin wax-graphene aerogel and indicated that graphene aerogel had an outstanding contribution to enhancing shape stability and heat conduction from 13.56 % to 44.44 % with the growth of reduction temperature. In addition, the paraffin wax-graphene aerogel composite displayed outstanding photothermal conversion capability [27].

N-heptadecne with outstanding features is a commercial phase change material, but its solid−liquid nature confined its practical applications [28] and to the best of our knowledge, there has been no report on the utilization of graphene, as a framework for n-heptadecane. Thereby, solid-solid stabilized n-heptadecane was fabricated using nanographene as a nanoskeleton material of n-heptadecane via an impregnation technique. The chemical structure, morphology, thermal properties, and heat conduction of

Table 1
N-heptadecne and nanographene compositions used for the fabrication of the n-heptadecane-graphene nanocomposites.

Nanocomposite	N-heptadecane content (%)	Ratio (N-heptadecane/Graphene)	N-heptadecane (g)	Graphene (g)
GND1	9.09	0.1	0.1	1
GND2	23.08	0.3	0.3	1
GND3	33.33	0.5	0.5	1
GND4	41.17	0.7	0.7	1
GND5	47.37	0.9	0.9	1

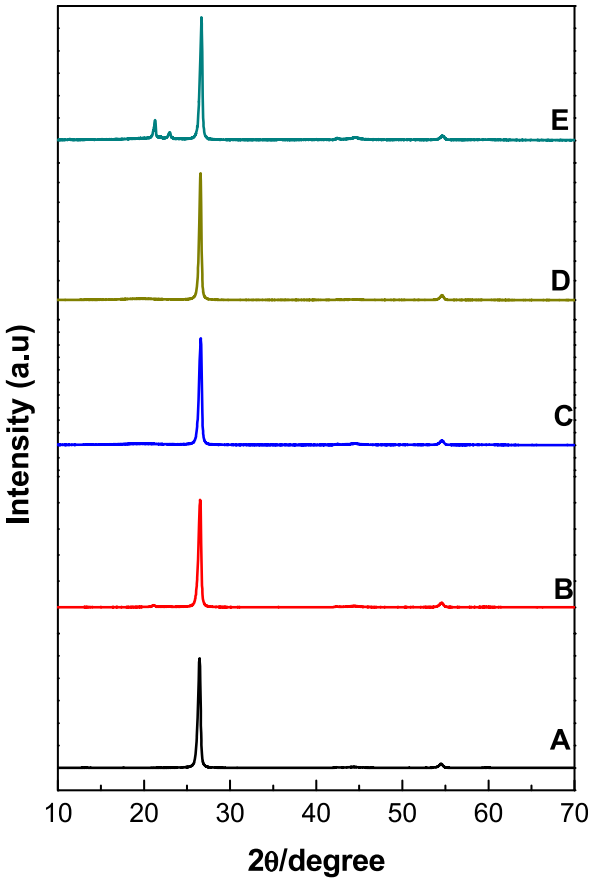

Fig. 2. Powder X-ray diffraction patterns for the graphene (**A**), GND1 nanocomposite (B), GND2 nanocomposite (C), GND3 nanocomposite (D), and GND4 nanocomposite (E).

prepared nanocomposites were investigated. Further, the thermal performance of the gypsum materials was elucidated after the incorporation of n-heptadecane-graphene nanocomposite.

2. Experimental section

2.1. Materials

Nanographene and n-heptadecane were obtained from Sigma-Aldrich (St Louis, MO, USA). Absolute ethanol was purchased from R&M Chemicals (UK). Gypsum and deionized water were used to produce the composites.

2.2. Preparation of n-heptadecane-graphene nanocomposite

N-heptadecane-graphene nanocomposites were prepared using a published procedure. The n-heptadecane was dissolved in 30 mL of absolute ethanol and then graphene was added slowly into the solution with stirring. The mixture was stirred for 4 h at room temperature and was then oven dried (Fig. 1). The PCM content in the nanocomposite was altered from 10 to 90 wt% and

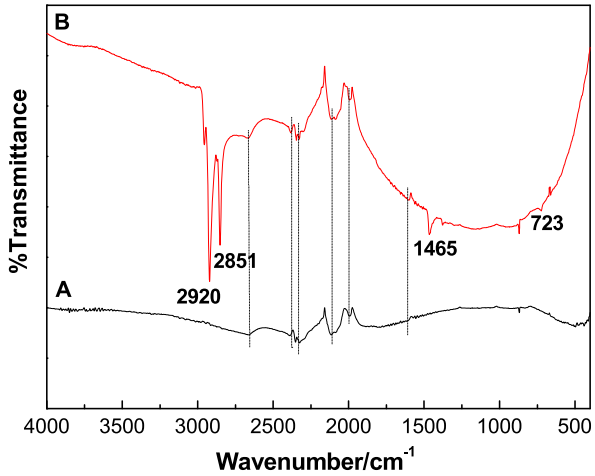

Fig. 3. Fourier transform infrared spectra of graphene (A) and GND4 nanocomposite (B).

nanocomposites were termed as GND1, GND2, GND3, GND4, and GND5 (Table 1).

2.3. Fabrication of the GND4 nanocomposite-gypsum composite boards

The gypsum composite boards holding 0.0, 6.0, and 9.0 wt% GND4 nanocomposite were made by combining 0.0, 4.8, and 7.2 g GND4 nanocomposite with 80.0, 75.2, and 72.8 g gypsum and 40 g water. The mixture was obtained by continuous combining with robust agitation for 4 min. Next, the prepared slurry was spilled into a mould 80 mm long, 80 mm wide, and 12 mm thick and was dried at ambient temperature. Subsequently, samples were put down and air-dried.

2.4. Characterization

Thermogravimetric and differential thermogravimetric analyses (TGA/DTG) of nanographene, n-heptadecane, and GND4 nanocomposite were performed on a Mettler Toledo instrument at a heating rate of 10 °C min^{-1} from 20 to 1000 °C under the N_2 atmosphere. The chemical compatibility and crystal structure of nanographene and n-heptadecane nanocomposites were studied via an X-ray diffraction (XRD) instrument (D8 ADVANCE, BRUKER, Germany) using Cu Kα radiation (λ = 0.154056 nm). The morphologies of nanographene and GND4 nanocomposite were visually characterized by an EM3900 M scanning electron microscope (SEM). The Fourier transform infrared (FTIR) spectroscopy measurements over the wavenumber region of 4000−400 cm^{-1} of nanographene and GND4 nanocomposite were attained by a Fourier transform infrared spectrometer (Thermo Scientific) with a resolution of 4 cm^{-1}. The phase change heat storage enthalpy test of nanographene, n-heptadecane, and GND4 nanocomposite was carried out by an 822e, Mettler Toledo differential scanning calorimeter (DSC) at a heating/cooling rate of 10 °C min^{-1}. The pore structure (BET-specific surface area and average pore diameter) of GND4 nanocomposite was studied by the N_2 gas adsorption-desorption method at 77 K, by an Accelerated Surface Area and Porosimeter (ASAP) (Micromeretic, 2000). The BET-specific surface area and pore size distribution of the nanocomposite were ascertained by the Brunauer-Emmet-Teller (BET) and Barrett-Joyner-Halenda (BJH) equations, respectively. Raman spectra of graphene and GND4 nanocomposite were measured by a Renishaw Raman spectrometer, cooled under liquid N_2. Raman wavenumbers were gained by a laser excitation wavelength at 514.5 nm.

3. Results and discussion

3.1. Chemical structure and compatibility of GND4 nanocomposite

The XRD patterns of graphene and GND nanocomposites at different n-heptadecane mass percentages were given in Fig. 2. Graphene was generally considered to be a 2D crystal (Mermin-Wagner theorem) made of just one layer of carbon atoms [29,30]. Its graphitic structure was proved by the XRD pattern (Fig. 2A) which displayed a dominant (002) Bragg peak at 26.38°, corresponding to an interlayer spacing of ~0.34 nm. The sharp diffraction peak at 26.38° with a high crystallinity designated that graphene has a good crystalline structure [31,32]. The two reflections at 21.22° and 23.04° were found in the XRD pattern of GND4 nanocomposite (Fig. 2E) were caused by n-heptadecane [33] and the intense peak of graphene also appeared at 26.38°. All diffraction peaks of GND4 nanocomposite fitted well with those of n-heptadecane and graphene. It was proposed that the GND4 nanocomposite was just the physical combination of n-heptadecane and graphene, and the structure of n-heptadecane was not destroyed upon the addition of graphene with no newly generated substance during integration as well. Nonetheless, no crystalline structure of n-heptadecane was detected for the GND nanocomposites containing below 50 wt% n-heptadecane (Fig. 2B–D). This might be a consequence of the small proportion of n-heptadecane in the graphene.

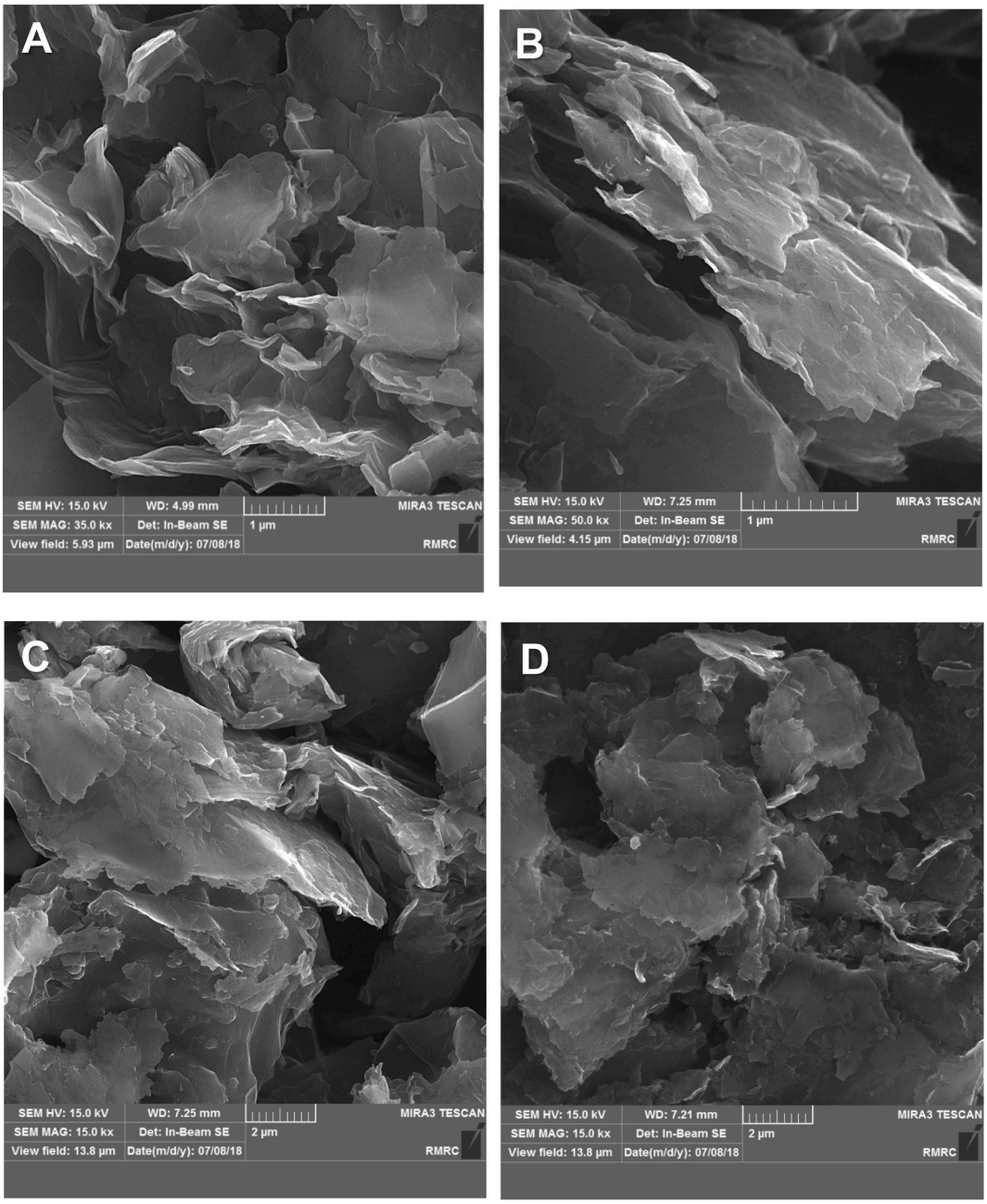

Fig. 4. SEM images of graphene (A) and GND4 nanocomposite (B–D).

To further explore the formation of the GND4 nanocomposite, the FTIR spectra of graphene and GND4 nanocomposite were demonstrated in Fig. 3. In the FTIR spectra of graphene (Fig. 3A), the C–H bonds which were located at the edge of the graphene sheet led to the characteristic absorption bands at 2672 cm^{-1}, 2325 cm^{-1}, and 2108 cm^{-1} while the stretching vibrations of C═C produced typical peaks at 1500–1800 cm^{-1} [34,35]. In the FTIR spectra of GND4 nanocomposite (Fig. 3B), the two strong absorption peaks at 2920 cm^{-1} and 2851 cm^{-1} were assigned to the asymmetric and symmetric stretching vibrations of C–H in $–CH_3$ and $–CH_2$ groups and the characteristic peaks at 1465 and 1375 cm^{-1} were bending vibrations of C–H in n-heptadcane. The absorption band at 723 cm^{-1} was caused by rocking and out-of-plane bending vibrations of CH_2 in n-heptadecane [36,37]. Additionally, the representative bands of graphene with no shifting in the peak position were observed in the GND4 nanocomposite. The absorption curves of the GND4 nanocomposite contained all characteristic peaks of both n-heptadecane and graphene without newly produced bands. Hence, it could be deduced that there was no chemical interaction between the graphene and n-heptadecane, as confirmed by the XRD results.

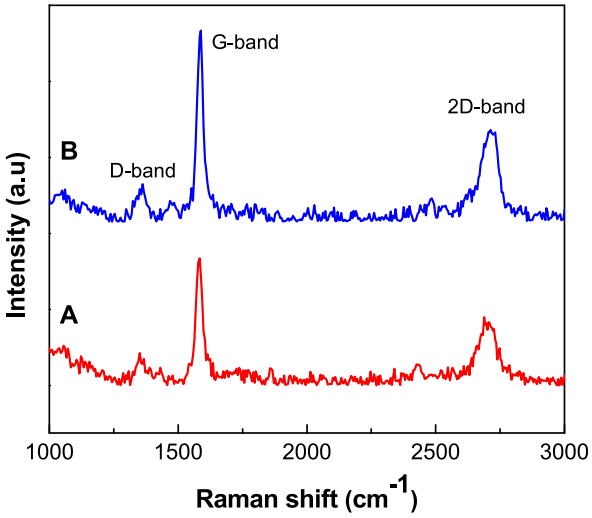

Fig. 5. Raman spectra of nanographene (A) and GND4 nanocomposite (B).

3.2. Surface morphology

Graphene is presently the thinnest renowned two-dimensional material and many of its special properties are attributed to its extreme thinness. Its well-known optical transparency is associated with its thinness. Besides, its excessive thinness and non-polar nature made graphene moderately transparent to van der Waals and electrostatic interactions as well [38,39]. As observed in Fig. 4A, the graphene nanosheets are wrinkled, transparent with smooth surfaces, and have a porous structure. Nonetheless, in GND4 nanocomposite the transparency is reduced due to the integration of n-heptadecane into the graphene pores and the graphene nanosheets appear thicker and darker (Fig. 4B–D). It is evident from SEM images of GND4 nanocomposite (Fig. 4B–D) that the n-heptadecane was well absorbed into the porous structure of the graphene by the surface tension between the n-heptadecane and graphene with no seepage problem which is beneficial for boosting thermal conductivity of GND4 nanocomposite.

3.3. Raman spectroscopy

Raman spectroscopy was used to further study the structure of GND4 nanocomposite, and the obtained spectra of graphene and GND4 nanocomposite were presented in Fig. 5. The typical peaks of graphene, denominated 2D, G, and D bands, were detected at 2688 cm^{-1}, 1583 cm^{-1}, and 1346 cm^{-1}, respectively (Fig. 5A). The defect is derived through the intensity ratio between the defect-induced D band and the Raman permitted identify band (ID/IG). Measuring defects in graphene is vital both to better comprehend their basic features and for utilization. The ID/IG ratio for graphene was 0.25 and a ratio of < 1, signifying lower disarrays and good aromatic structure of graphene [40,41]. However, in the GND4 nanocomposite Raman spectrum (Fig. 5B) three main peaks were observed at 2714 cm^{-1}, 1588 cm^{-1}, and 1362 cm^{-1} corresponded to 2D, G, and D bands, respectively, and the ID/IG ratio for GND4 nanocomposite was 0.56.

3.4. Thermal stability

Diverse applications required PCM nanocomposites to have varied thermal stability, thus it was essential to probe the thermal stability features. The thermal stability of nanographene, n-heptadecane, and GND4 nanocomposite was studied via thermogravimetric and differential thermogravimetric (TGA/DTG), and the results were displayed in Fig. 6. Graphene gave only a degradation peak at 158 °C which could be assigned to the removal of water molecules (Fig. 6A). The degradation temperature of n-heptadecane was 230 °C corresponding to the vaporization of n-heptadecane (Fig. 6B) though the GND4 nanocomposite had a similar degradation step to pure PCM that was due to the vaporization of n-heptadecane inside the GND4 nanocomposite (Fig. 6C). Consequently, the GND4 nanocomposite remained constant at operation temperature with appropriate practical functions.

3.5. Porosity structure and surface area

The porosity and surface area of GND4 nanocomposite were examined using N_2 adsorption-desorption isotherm measurements. GND4 nanocomposite exhibited a type IV isotherm with an H3-hysteresis loop related to a mesoporous structure [42]. In the GND4 nanocomposite in Fig. 7A, N_2 adsorption in low relative pressure ($P/P_0 < 0.7$) was seldom observed, and inversely, in the comparatively high-pressure area ($P/P0 > 0.7$), it showed an abrupt adsorption point, and an H3-type hysteresis loop appeared. This type of isotherm and hysteresis were mostly shown by parallel walls and narrow neck capillaries. Thus, it could be observed that most of the

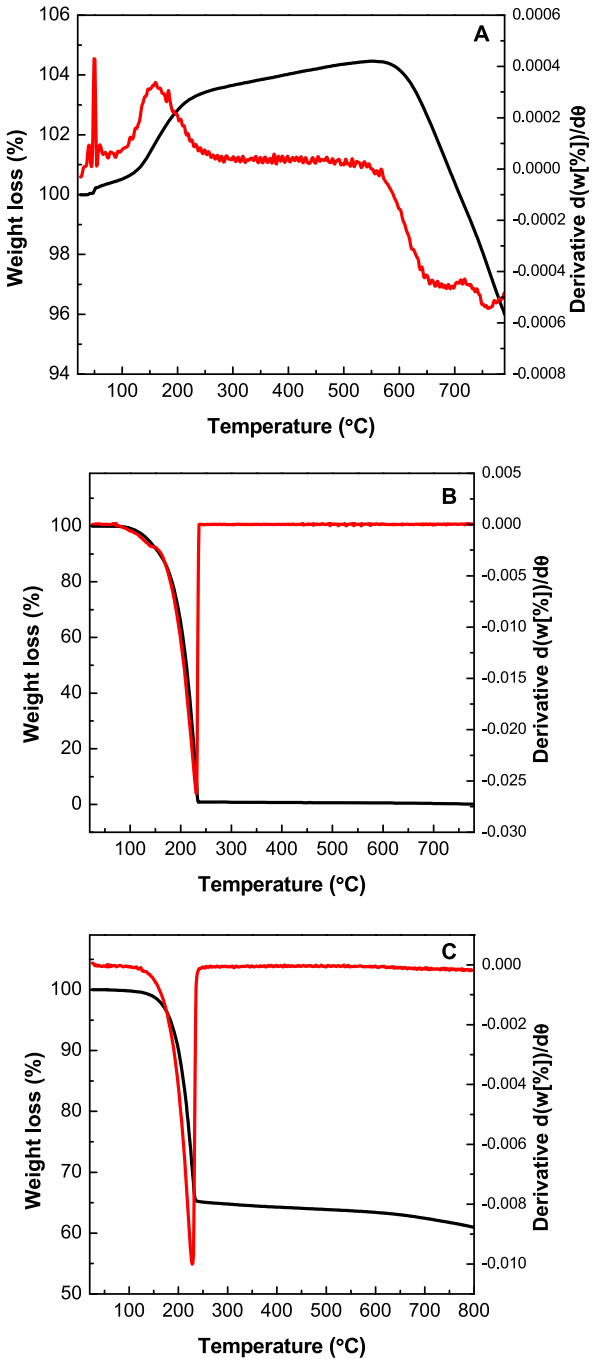

Fig. 6. Thermogravimetric and differential thermogravimetric (TGA/DTG) thermograms of nanographene (A), n-heptadecane (B), and GND4 nanocomposite (C).

pores of GND4 nanocomposite were slit-shaped pores slit by the aggregation of nanosheets. The surface area and pore size distribution of GND4 nanocomposite were determined using the Brunauer, Emmett, and Teller (BET) and Barrett–Joyner–Halenda (BJH) methods, respectively. It had a BJH average pore diameter of 20 nm (Fig. 7B) and a BET-specific surface area of 13 m^2/g.

3.6. Phase-change properties

Energy storage capacity is a crucial parameter for PCM nanocomposites and is usually characterized by latent heat derived from the phase change process. The latent heat of graphene, n-heptadecane, and GND4 nanocomposite in both melting and freezing procedures,

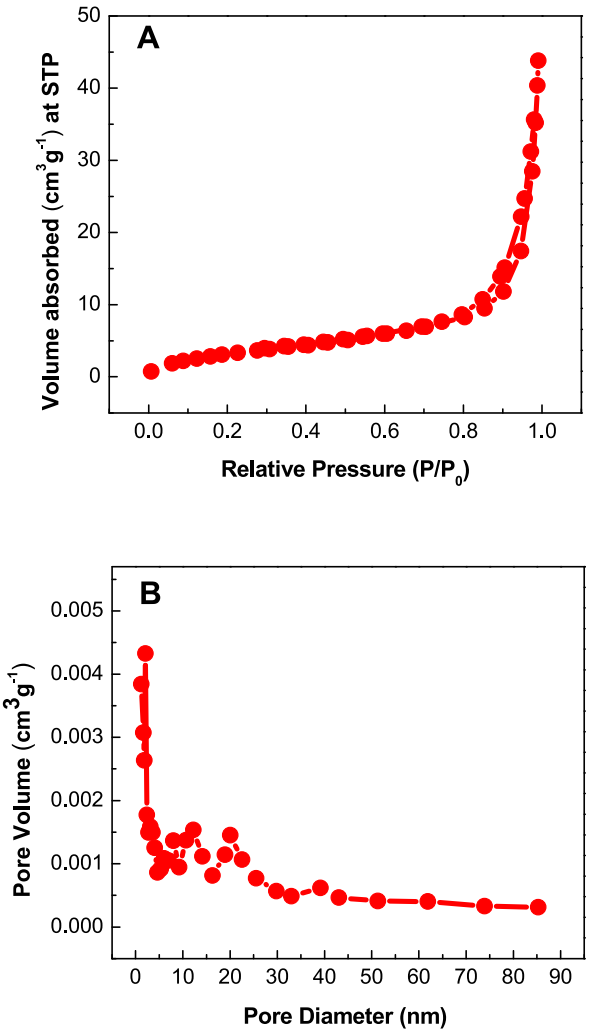

Fig. 7. N2 Adsorption-desorption isotherm (A) and BJH desorption pore size distribution (B) of GND4 nanocomposite.

as well as phase change temperature, were measured using DSC analysis, as demonstrated in Fig. 8. In Fig. 8B and C, the solid-liquid and liquid-solid phase transitions peaks for pure n-heptadecane and GND4 nanocomposite exhibited that the heat absorbing and releasing processes were taken place. The absence of the peaks observed in the graphene (Fig. 8A) was due to the absence of n-heptadecane. The melting-cooling characteristics of the GND4 nanocomposite were similar to those of pure n-heptadecane. The DSC curves of pure n-heptadecane indicated obvious exothermic and endothermic peaks at 17.1 °C and 24.6 °C, respectively, while the melting enthalpy (ΔH_m) and crystallization enthalpy (ΔH_c) were 222.9 and 222.1 J/g, respectively. The GND4 nanocomposite displayed exothermic and endothermic peaks at 15.0 °C and 27.0 °C, with the latent heat of 101.3 and 101.7 J/g, during melting and freezing, respectively, according to the DSC curves of GND4 nanocomposite.

The phase change temperature and the energy storage efficiency of GND4 nanocomposite were determined by the n-heptadecane content in the GND4 nanocomposite, hence, the incorporated rate (wt.%) of n-heptadecane in the framework of nanographene was calculated using the following formula (equation (1)):

$$Incoporated\ rate(wt\%) = \frac{\Delta H_{m,GND4} + \Delta H_{c,GND4}}{\Delta H_{m,PCM} + \Delta H_{c,PCM}} \times 100 \quad (1)$$

where $\Delta H_{m,GND4}$ and $\Delta H_{c,GND4}$ were the melting enthalpy and the freezing enthalpy of the GND4 nanocomposite and $\Delta H_{m,PCM}$ and $\Delta H_{c,PCM}$ were the melting enthalpy and the crystallization enthalpy of the pure n-heptadecane, respectively [43].

The n-heptadecane content in the GND4 nanocomposite from DSC data was found to be 45.6 % which was consistent well with the weight loss of GND4 nanocomposite recorded TGA/DTG.

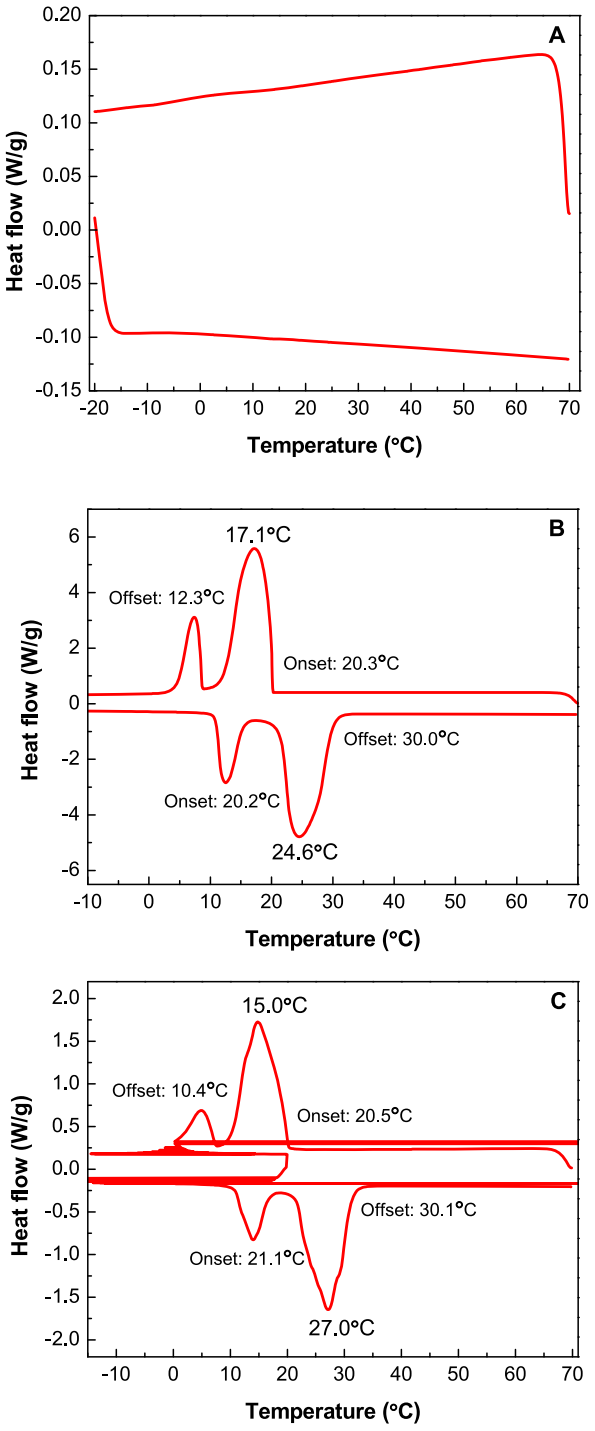

Fig. 8. DSC curves of nanographene (A), n-heptadecane (B), and GND4 nanocomposite (C).

3.7. Thermal conduction

Heat conduction was the critical factor for the efficiency of energy storing and releasing in the practical implementation of heat storage systems and thermal management. Heat conduction measurements were conducted on a heat conduction device (KD-2 Pro), via the hot wire technique. The heat conductivities of the pristine n-heptadecane, GND1, GND2, GND3, GND4, and GND5 nanocomposites were 0.168 W/mK, 0.991 W/mK, 1.527 W/mK, 1.931 W/Mk, 2.503 W/Mk, and 7.512 W/Mk, respectively (Fig. 9). With a rising amount of nanographene added, the heat conduction of the GND nanocomposites steadily enhanced (Fig. 9). The improvement

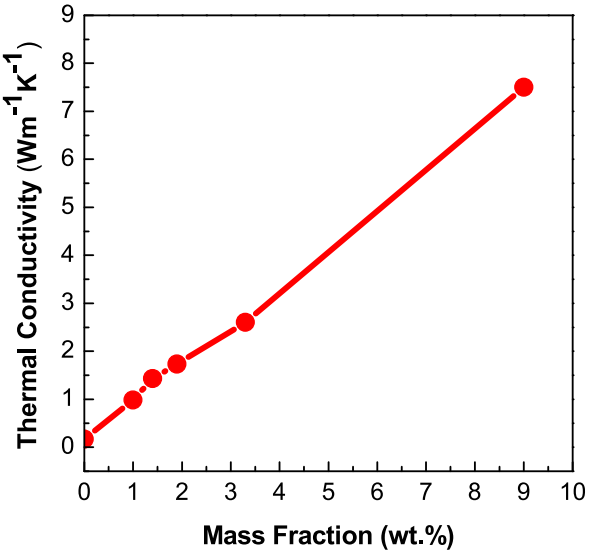

Fig. 9. Thermal conductivity of n-heptadecane and GND nanocomposites.

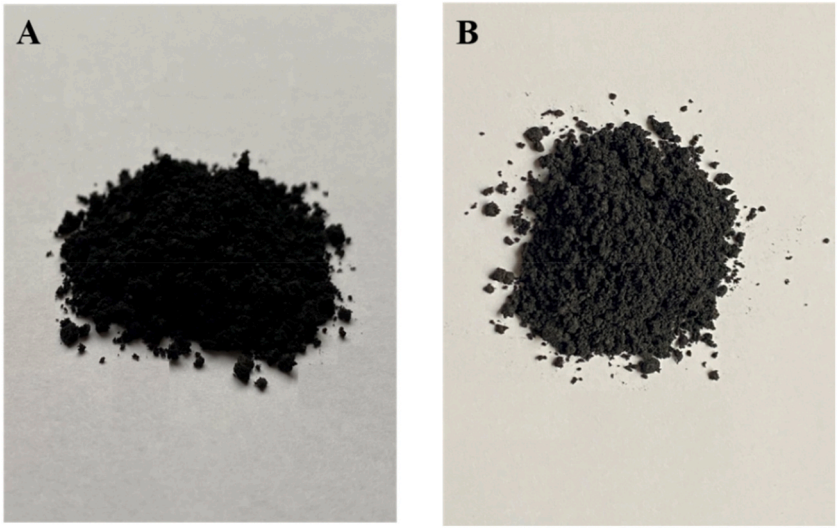

Fig. 10. GND4 nanocomposite before (A) and after the leaching test (B).

in heat conduction of GND nanocomposites could be related to the good interface, extraordinary thermal conductivity value, and synergistic effect of graphene. Notably, the measurements proved that graphene acted as an efficient nanoskeleton to transfer its inherent heat conductivity into GND nanocomposites.

3.8. Shape stability of GND4 nanocomposite

The leakage test was done to evaluate the ability of graphene as a framework to maintain the n-heptadecane throughout the melting process. This analysis was carried out by placing the GND4 nanocomposite in the oven at 75 °C for 24 h. 1.0002 g of the GND4 nanocomposite (Fig. 10A) was weighed and put on filter paper before the leakage test. Subsequently, it was conditioned at 22 °C for 7 h to examine the capability of graphene to maintain n-heptadecane throughout the melting phase. No greasy property of n-heptadecane was seen on the filter paper. Afterward, the GND4 nanocomposite was subjected to 75 °C for 48 h. The aim of this analysis was to clarify the ability of the graphene to maintain n-heptadecane with no seepage at temperatures above the melting temperature of n-heptadecane. No liquid spillage was detected after the nanocomposite was subjected to temperatures higher than the melting point of n-heptadecane and the weight of the nanocomposite after the leakage test was 0.9982 g (Fig. 10B). This result expressed that the n-heptadecane favourably permeated graphene, and the graphene structure afforded adequate capillary and adsorption forces to avoid

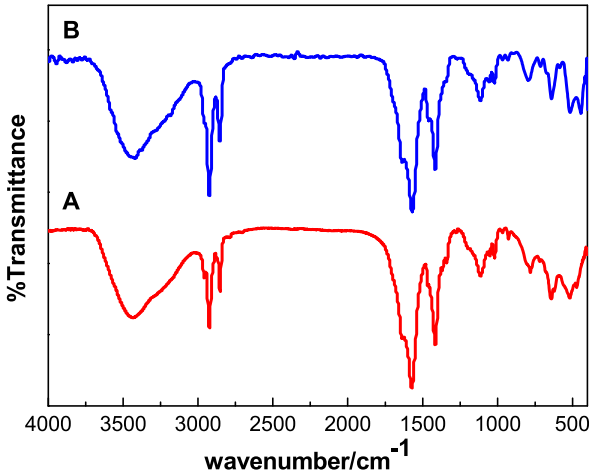

Fig. 11. FTIR spectra of GND4 nanocomposite before (A) and after 400 thermal cycles (B).

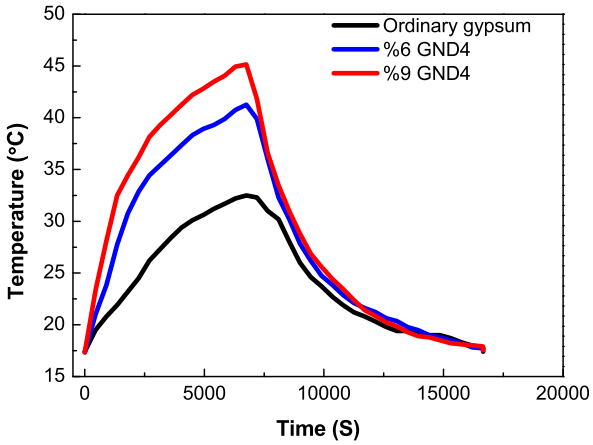

Fig. 12. External surface temperature graphs of the gypsum composite boards contained 0.0, 6.0, and 9.0 wt% of GND4 nanocomposite.

leakage of the melted n-heptadecane.

3.9. Thermal reliability

A heat cycle test was accomplished to evaluate the features of the GND4 nanocomposite in terms of its reversibility of heat storage and chemical stability after several heat cycles. A heat cycle test was performed for 400 cycles for the nanocomposite and no seepage of n-heptadecane from the GND4 nanocomposite was seen throughout the heat cycle test. The chemical stability of the GND4 nanocomposite prior to and afterward the thermal cycling test was demonstrated in Fig. 11 (A and B). There was no substantial change in the shape and frequency values of all of the peaks after 400 heat cycles. This outcome expressed that the chemical structure of the GND4 nanocomposite was not influenced by the recurred thermal cycles. Comparable results were also stated for nonadecane-SiO_2-graphene nanocomposite [35], paraffin-silica nanocomposite [44], n-heptadecane-SiO_2 nanocomposite [33], and eutectic of paraffin wax and palmitic acid-TiO_2 nanocomposite [45]. Hence, the GND4 nanocomposite is suitable to be utilized for energy storage.

3.10. Thermal behaviour of GND4 nanocomposite gypsum composite

The thermal performance estimations of the gypsum composite boards were accomplished by insertion a lamp (500 W) above the gypsum composite boards at a distance of 25.0 cm. Throughout the test, the environment temperature was retained at 20 ± 3 °C. Fig. 12 displayed the external surface temperature curves for the gypsum composite boards containing 0.0, 6.0, and 9.0 wt% GND4 nanocomposite when exposed to heating and cooling. Under light irradiation, the temperature of samples rose quickly in proportion to the content of GND4 nanocomposites, as presented in Fig. 12. This performance was associated with the good heat conduction of the GND4 nanocomposite. The temperature of ordinary gypsum increased quite slowly (maximum temperature of 33 °C) under light irradiation, due to the low heat conduction of gypsum. Although reuniting with GND4 nanocomposite, samples had effective heat

Table 2
Comparison of thermoregulation property of GND4 nanocomposite with literature.

PCM	Framework	Latent heat of PCM nanocomposite/ composite (J/g)	Thermal conductivity (W/mK)	Thermal cycles	Performance in gypsum	Reference
Stearic acid-*n*-nonadecane	SiO_2 nanoparticles	86.5	–	500	Composite maintained the interior temperature in the human comfort region and reduced energy demand.	[46]
Paraffin	Poly methacrylate	–	0.139	–	The PCM composite had 1.5 °C higher temperature and 0.4 W/min higher retained energy than the gypsum plasterboard.	[47]
Capric acid–palmitic acid	Urea-formaldehyde	189.7	0.1854	–	The composite with 10 wt% PCM microcapsules indicated promise as a material for practical applications.	[48]
1-dodecanol	Attapulgite	115.9	0.182	–	The interior temperatures of the small testing room made of 1-dodecanol-attapulgite-gypsum were around 1.2 °C-2.7 °C warmer than that of the gypsum room for around 6–12 h in the winter.	[49]
Palm oil	Barley straws	59.10	0.328	–	The gypsum composite with the ratio of 2.6:1.0 enhanced the heat transfer rate, with a lessening of 12.1 % in comparison with the basic composition, and showed good chemical stability.	[50]
lauric acid	Zeolite -graphite	81.08	0.242	1000	Incorporating lauric acid zeolite-graphite in the gypsum enhanced the inside temperature trend of the building.	[51,52]
Microencapsulated PCM	Glass fiber-gypsum	203.0	0.422	300	High thermally stable gypsum plasterboard diminished the cooling demand of a house throughout the day even at the high room temperature and offered a decrease in the heat demand of a room throughout the night.	[53,54]
N-octadecane	Expanded vermiculite, expanded perlite, nano carbon	–	0.325, 0.294, 0.272, 0.283	–	All gypsum boards with PCM improved the resident's comfort through effectual moisture and temperature regulation, reduced energy consumption, and had better hygro-thermal performance and energy saving.	[55]
N-heptadecane	SiO_2 nanoparticles	123.8	0.2835	500	Gypsum composite boards showed acceptable temperature control performance with maximum temperature differences of 1.0 °C, 3.8 °C and 5.7 °C in 2 h for gypsum wallboards containing 0.0, 1.0, 4.0, and 8.0 wt% nanocomposite, respectively.	[33]
SAT-urea eutectic salts	Activated carbon	103.0	0.3079	100	The PCM-activated carbon slowly reduced the heat conduction and considerably enhanced the heat capacity of the gypsum composites	[56]
Lauryl alcohol-stearic acid	Diatomite	67.72	0.2515	400	Lauryl alcohol-stearic acid-diatomite-gypsum board demonstrated adequate functioning relating to the thermal energy saving and temperature delay, extenuating temperature variations interior, and humidity absorption compared with the normal gypsum.	[57]
Paraffin	Calcium sulfate whisker	21.31	–	–	The gypsum comprising 15.0 wt% PA had the best features and the composites with 3.5 wt% CSW content, their compressive strength and flexural were improved by 278.0 % and 131.0 %, respectively.	[58]
N-heptadecane	Graphene	101.7	1.527	300	Integration of the mesoporous nanocomposite in the gypsum boards (containing 6.0 and 9.0 wt% GN4 nanocomposite) decreased energy uptake and controlled building temperature by slower heat release rate than the gypsum-only board.	This work

absorption upon light irradiation, and the temperature of samples escalated rapidly with a maximum temperature of 42 °C, and 46 °C for the gypsum composite board containing 6.0, and 9.0 % GND4 nanocomposite, respectively. When the lamp was turned off, the temperature of all the samples dropped but the heat release rate of the gypsum board containing 6.0, and 9.0 % GND4 nanocomposites was swifter than only the gypsum board. The consequence revealed that the GND4 nanocomposite had proper chemical and thermal stability, and with appropriate heat absorption and release rate acted as thermal energy storage even after integration in gypsum.

3.11. Comparing of heat regulating performance of GND4 nanocomposite with prior research

In previous findings, it is feasible to run across several studies about the thermal functionality of wallboards or plasterboards created with PCM-gypsum/PCM nanocomposite-gypsum on a lab-scale designed unit. A majority of the literature exhibited that the gypsum composite could diminish indoor temperature fluctuations (Table 2).

Nevertheless, the outputs of this study were accorded well with the aforementioned works.

4. Conclusion

A novel shape-stable and solid-solid PCM was produced through a simple impregnation process using nanographene as a nanoscale material, and n-heptadecane as a solid-liquid phase-change functional material. This mesopore GND4 nanocomposite presented appropriate thermal conduction (1.527 W/mK) and could be assigned to the construction of the 2D heat transfer network of graphene in the n-heptadecane matrix. The melting and freezing of the optimized nanocomposite were observed at 27.0 °C with a phase change enthalpy of 101.7 J/g and 15.0 °C with a phase change enthalpy of 101.3 J/g, respectively**.** The leakage test indicated that the thermally stable nanocomposite containing 45.6 % n-heptadecane could maintain a solid form without seepage in the melting state of n-heptadecane and after 400 thermal cycles, the thermal reliability test depicted that the GND4 nanocomposite possessed desirable thermal reliability. Furthermore, integrating GND4 nanocomposite in the gypsum boards reduced energy consumption and decreased building temperature fluctuations by swift heat release rate. Therefore, the GND4 nanocomposite might be considered a suitable applicant for energy storage in building energy efficacy.

Data availability statement

Data will be made available on request.

Additional information

No additional information is available for this paper.

CRediT authorship contribution statement

Mohadeseh Amirkhani Khabisi: Methodology, Funding acquisition, Data curation. **Ghodratollah Roudini:** Supervision, Funding acquisition, Conceptualization. **Farahnaz Barahuie:** Writing – review & editing, Writing – original draft, Validation, Supervision, Methodology, Investigation, Formal analysis, Data curation, Conceptualization. **Hamed Sheybani:** Methodology, Funding acquisition, Formal analysis. **Muhammad Ibrar:** Formal analysis.

Declaration of competing interest

The authors declare that they have no known competing financial interests or personal relationships that could have appeared to influence the work reported in this paper.

References

[1] K. Liu, Z.F. Yuan, H.X. Zhao, C.H. Shi, F. Zhao, Properties and applications of shape-stabilized phase change energy storage materials based on porous material support—a review, Mater. Today Sustain. 21 (2023), 100336.
[2] H. Christen, S. Cho, G.v. Zijl, W.d. Villiers, Phase change material infused recycled brick aggregate in 3D printed concrete, Heliyon 8 (2022), e11598.
[3] Z. Zhang, Y. Liu, W. Du, Z. Liang, F. Li, Y. Yong, Z. Li, Construction of layered double hydroxide-modified silica integrated multilayer shell phase change capsule with flame retardancy and highly efficient thermoregulation performance, J. Colloid Interface Sci. 632 (2023) 311–325.
[4] P. Sukontasukkul, T. Sangpet, M. Newlands, D.-Y. Yoo, W. Tangchirapat, S. Limkatanyu, P. Chindaprasirt, Thermal storage properties of lightweight concrete incorporating phase change materials with different fusion points in hybrid form for high-temperature applications, Heliyon 6 (2020), e04863.
[5] Q. He, H. Fei, J. Zhou, X. Liang, Y. Pan, Utilization of carbonized water hyacinth for effective encapsulation and thermal conductivity enhancement of phase change energy storage materials, Constr. Build. Mater. 372 (2023), 130841.
[6] M.S. Mondal, S.Z. Hussain, M. Ullah, A facile synthesis approach of silica aero-gel/eicosane particles and its potential application on polyester fabric to impart thermoregulation properties, Heliyon 9 (2023), e12935.
[7] S. Tan, X. Zhang, Progress of research on phase change energy storage materials in their thermal conductivity, J. Energy Storage 61 (2023), 106772.
[8] D. Karimi, M.S. Hosen, H. Behi, S. Khaleghi, M. Akbarzadeh, J.V. Mierlo, M. Berecibar, A hybrid thermal management system for high power lithium-ion capacitors combining heat pipe with phase change materials, Heliyon 7 (2021), e07773.
[9] P. Singh, R.K. Sharma, M. Khalid, R. Goyal, A. Sarı, V.V. Tyagi, Evaluation of carbon based-supporting materials for developing form-stable organic phase change materials for thermal energy storage: a review, Sol. Energy Mater. Sol. Cells 246 (2022), 111896.

[10] L. Jiang, L. Zhao, G. Chen, M. Li, R. Zhang, Graphite-enhanced thermal properties of octadecylamine/graphite foam shape-stable composite phase change materials for thermal energy storage, Energy Rep. 8 (2022) 13939–13947.
[11] X. Zhao, C. Li, K. Bai, B. Xie, J. Chen, Q. Liu, Multiple structure graphite stabilized stearic acid as composite phase change materials for thermal energy storage, Int. J. Min. Sci. Technol. 32 (2022) 1419–1428.
[12] Y. Zhao, K. Zhang, X. Min, J. Xiao, Z. Xu, Z. Huang, Y. Liu, X. Wu, M. Fang, Graphene aerogel stabilized phase change material for thermal energy storage, Case Stud. Therm. Eng. 40 (2022), 102497.
[13] W. Su, M. Hu, L. Wang, G. Kokogiannakis, J. Chen, L. Gao, A. Li, C. Xu, Microencapsulated phase change materials with graphene-based materials: fabrication, characterisation and prospects, Renew. Sustain. Energy Rev. 168 (2022), 112806.
[14] M. Ghalambaz, S.M. Hashem Zadeh, S.A.M. Mehryan, A. Haghparast, H. Zargartalebi, Free convection of a suspension containing nano-encapsulated phase change material in a porous cavity; local thermal non-equilibrium model, Heliyon 6 (2020), e03823.
[15] S. Tanwar, R. Kaur, Fabrication and investigation on influence of metal oxide nanoparticles on thermal, flammability and UV characteristics of polyethylene glycol based phase change materials, J. Energy Storage 54 (2022), 105318.
[16] E. Tangsiriratana, W. Skolpap, R.J. Patterson, K. Sriprapha, Thermal properties and behavior of microencapsulated sugarcane wax phase change material, Heliyon 5 (2019), e02184.
[17] L. Hu, Y. An, L. Zhang, L. Mai, T. Ma, Q. An, Q. Wang, Shape-stabilized phase change material based on MOF-derived oriented carbon nanotubes for thermal management of lithium-ion battery, J. Energy Storage 72 (2023), 108520.
[18] S. Niu, M. Kang, Y. Liu, W. Lin, C. Liang, Y. Zhao, J. Cheng, The preparation and characterization of phase change material microcapsules with multifunctional carbon nanotubes for controlling temperature, Energy 268 (2023), 126652.
[19] K. Wang, R. Wen, Scaphium scaphigerum/graphene hybrid aerogel for composite phase change material with high phase change enthalpy and high thermal conductivity for energy storage, J. Energy Storage 58 (2023), 106302.
[20] T.T. Tung, M.T. Tran, A.L.C. Pereira, C.M.B. Cordeiro, D.D. Nguyen, N.-H. Tai, V.V. Tran, C.C. Hsu, P. Joshi, M. Yoshimura, J.F. Feller, M. Castro, K. Hassan, M. J. Nine, N. Stanley, D. Losic, Graphene woven fabric-polydimethylsiloxane piezoresistive films for smart multi-stimuli responses, Colloids Surf. B Biointerfaces 221 (2023), 112940.
[21] A.L. Olatomiwa, T. Adam, C.O. Edet, A.A. Adewale, A. Chik, M. Mohammed, S.C.B. Gopinath, U. Hashim, Recent advances in density functional theory approach for optoelectronics properties of graphene, Heliyon 9 (2023), e14279.
[22] Y. Cai, N. Zhang, X. Cao, Y. Yuan, Z. Zhang, N. Yu, Ultra-light and flexible graphene aerogel-based form-stable phase change materials for energy conversion and energy storage, Sol. Energy Mater. Sol. Cells 252 (2023), 112176.
[23] L. Jiang, G. Chen, L. Zhao, M. Li, C. Li, R. Zhang, Preparation and low temperature heat storage properties of 1-hexadecylamine/3Dgraphene aerogel composite phase change materials, Sol. Energy Mater. Sol. Cells 251 (2023), 112118.
[24] S. Khanna, S. Paneliya, P. Prajapati, R. Chaudhari, J. Vora, H. Jouhara, Investigating the thermal properties of *n*-hexacosane/graphene composite: a highly stable nanocomposite material for energy storage application, Therm. Sci. Eng. Prog. 39 (2023), 101712.
[25] S. Hasbi, N. Norazman, M.S. Saharudin, Effects of titanium oxide and graphene as nano-fillers on the thermal conductivity of biobased phase change materials as latent thermal heat storage, Mater. Today: Proceed. 75 (2023) 181–187.
[26] P. Yang, B. Wu, X. Tong, M. Zeng, Q. Wang, Z. Cheng, Insight into heat transfer process of graphene aerogel composite phase change material, Energy 279 (2023), 128051.
[27] M. He, D. Xie, L. Yin, K. Gong, K. Zhou, Influences of reduction temperature on energy storage performance of paraffin wax/graphene aerogel composite phase change materials, Mater. Today Commun. 34 (2023), 105288.
[28] G. Hekimoğlu, A. Sarı, S. Arunachalam, H. Arslanoglu, O. Gencel, Porous biochar/heptadecane composite phase change material with leak-proof, high thermal energy storage capacity and enhanced thermal conductivity, Powder Technol. 394 (2021) 1017–1025.
[29] M.I. Katsnelson, A. Fasolino, Graphene as a prototype crystalline membrane, Acc. Chem. Res. 46 (2013) 97–105.
[30] Z. Dehghani, F. Ostovari, S. Sharifi, A comparison of the crystal structure and optical properties of reduced graphene oxide and aminated graphene nanosheets for optoelectronic device applications, Optik 274 (2023), 170551.
[31] L. Rao, Z. Zhou, H. Liu, W. Peng, Y. Li, F. Zhang, X. Fan, In-situ electrochemical conversion of $Na_5V_{12}O_{32}$@graphene for enhanced cycle stability in aqueous zinc ion batteries, J. Colloid Interface Sci. 629 (2023) 473–481.
[32] C.M. Kurmarayuni, B. Chandu, L.P. Yangalasetty, S.J. Gali, M.M. Alam, P.P. Rani, H.B. Bollikolla, Sustainable synthesis of silver decorated graphene nanocomposite with potential antioxidant and antibacterial properties, Mater. Lett. 308 (2022), 131116.
[33] S. Golestani Ranjbara, G. Roudinia, F. Barahuie, Fabrication and characterization of phase change material-SiO2 nanocomposite for thermal energy storage in buildings, J. Energy Storage 27 (2020), 101168.
[34] Y. Xu, Y. Chu, T. Zhao, X.R. Liu, C. Shen, L. Dong, L. Cui, Y. Shen, W.-S. Li, F.-G. Zhao, Engineering electronic structure of graphene to boost Lithium-Storage performance, J. Colloid Interface Sci. 640 (2023) 383–390.
[35] S.M. Musavi, F. Barahuie, M. Irani, A. Safamanesh, Enhanced properties of phase change material -SiO2-graphene nanocomposite for developing structural-functional integrated cement for solar energy absorption and storage, Renew. Energy 174 (2021) 918–927.
[36] J. Li, L. Jia, Y. Chen, L. Li, S. Mo, J. Wang, C. Wang, Microfluidic fabrication and thermal properties of microencapsulated n-heptadecane with hexanediol diacrylate shell for thermal energy storage, Appl. Therm. Eng. 162 (2019), 114278.
[37] D. Sarabandi, G. Roudini, F. Barahuie, Activated carbon derived from pine cone as a framework for the preparation of n-heptadecane nanocomposite for thermal energy storage, J. Energy Storage 24 (2019), 100795.
[38] D. Ghoshal, R. Jain, N.A. Koratkar, Graphene's partial transparency to van der waals and electrostatic interactions, Langmuir 35 (2019) 12306–12316.
[39] S. Chae, S. Jang, W.J. Choi, Y.S. Kim, H. Chang, T.I. Lee, J.-O. Lee, Lattice transparency of graphene, Nano Lett. 17 (2017) 1711–1718.
[40] R. Fates, R. Remmouche, T. Benkedidah, J.-P. Raskin, Evolution of the Raman spectra features of defective monolayer graphene in back-gate configuration: experimental study, Diam. Relat. Mater. 136 (2023), 109919.
[41] X. Fu, X. Dong, G. Yang, S. Bai, Non-isothermal crystallization kinetics of graphene/PA10T composites, Heliyon 8 (2022), e10206.
[42] X. Wang, H. Cheng, P. Chai, J. Bian, X. Wang, Y. Liu, X. Yin, S. Pan, Z. Pan, Pore characterization of different clay minerals and its impact on methane adsorption capacity, Energy Fuels 34 (2020) 12204–12214.
[43] W. Li, D. Zhai, Y. Gu, Y. Cao, L. Zhang, X. Sheng, Y. Chen, 3D zirconium phosphate/polyvinyl alcohol composite aerogels for form-stable phase change materials with brilliant thermal energy storage capability, Sol. Energy Mater. Sol. Cells 239 (2022), 111681.
[44] P.T. Saravanakumar, S.P. Arunkumar, B.B. Mansingh, P.M. Kumar, R. Subbiah, V.K. Eswarlal, Investigating the effect of thermal cycling on thermal characteristics of the nano-silica based phase changing material (PCM), Mater. Today: Proceed. 50 (2022) 1502–1507.
[45] J. Jacob, A.K. Pandey, N. Abd Rahim, J. Selvaraj, J. Paul, M. Samykano, R. Saidur, Quantifying thermophysical properties, characterization, and thermal cycle testing of nano-enhanced organic eutectic phase change materials for thermal energy storage applications, Sol. Energy Mater. Sol. Cells 248 (2022), 112008.
[46] S.M. Musavi, G. Roudini, F. Barahuie, S.M. Binti Masuri, Thermal energy storage property and temperature control performance of phase change materials eutectic mixture nanocomposite, Micro Nanosyst. 14 (2022) 272–280.
[47] M. Bake, A. Shukla, S. Liu, Development of gypsum plasterboard embodied with microencapsulated phase change material for energy efficient buildings, Mater. Sci. Energy Technol. 4 (2021) 166–176.
[48] C. Chen, L. Fang, Y. Wang, S. Jiu, Y. Chen, Mechanical, thermal and microscopic properties of gypsum matrix composites containing capric acid-palmitic acid/urea-formaldehyde microcapsules, Case Stud. Constr. Mater. 18 (2023), e02084.
[49] A. Yaras, A. Ustaoglu, O. Gencel, A. Sarı, G. Hekimoglu, M. Sutcu, E. Erdogmus, G. Kaplan, O.Y. Bayraktar, Characteristics, energy saving and carbon emission reduction potential of gypsum wallboard containing phase change material, J. Energy Storage 55 (2022), 105685.
[50] K. Kehli, B. Belhadj, A. Ferhat, Development of a new lightweight gypsum composite: effect of mixed treatment of barley straws with hot water and bio-based phase change material on the thermo-mechanical properties, Constr. Build. Mater. 389 (2023), 131597.

[51] N. Kumar, P.K.S. Rathore, R.K. Sharma, N.K. Gupta, Integration of lauric acid/zeolite/graphite as shape stabilized composite phase change material in gypsum for enhanced thermal energy storage in buildings, Appl. Therm. Eng. 224 (2023), 120088.
[52] N. Kumar, P.K.S. Rathore, A.K. Pal, Experimental investigation of composite gypsum board integrated with phase change material for improved thermal energy storage, Mater. Today: Proceed. 80 (2023) 1573–1578.
[53] O. Gencel, G. Hekimoglu, A. Sarı, A. Ustaoglu, S. Subasi, M. Marasli, E. Erdogmus, S.A. Memon, Glass fiber reinforced gypsum composites with microencapsulated PCM as novel building thermal energy storage material, Constr. Build. Mater. 340 (2022), 127788.
[54] O. Gencel, M. Bayram, S. Subası, G. Hekimoglu, A. Sarı, A. Ustaoglu, M. Marasli, T. Ozbakkaloglu, Microencapsulated phase change material incorporated light transmitting gypsum composite for thermal energy saving in buildings, J. Energy Storage 67 (2023), 107457.
[55] Ji Hun Park, Yujin Kang, Jongki Lee, Wi Seunghwan, J.D. Chang, Sumin Kim, Analysis of walls of functional gypsum board added with porous material and phase change material to improve hygrothermal performance, Energy Build. 183 (2019) 803–816.
[56] C. Chen, X. Wang, F. Ma, Y. Wang, S. Jiu, Y. Chen, Preparation and characterization of modified activated carbon-based shape stabilized eutectic phase change materials for gypsum composites application, Constr. Build. Mater. 369 (2023), 130551.
[57] Y. Yang, Z. Shen, W. Wu, H. Zhang, Y. Ren, Q. Yang, Preparation of a novel diatomite-based PCM gypsum board for temperature-humidity control of buildings, Build. Environ. 226 (2022), 109732.
[58] F. Ma, C. Chen, Y. Wang, Mechanical behavior of calcium sulfate whisker-reinforced paraffin/gypsum composites, Constr. Build. Mater. 305 (2021), 124795.